Research Article | Vol. 30, No. 16 / 1 Aug 2022 / Optics Express 28745
Optics EXPRESS

Direct generation of orbital angular momentum in orthogonal fiber Bragg grating

RUI LIU,[1,2,3] YALI LI,[1,2,3] JIAYAN CHEN,[1,2] LUPING WU,[1,2] JIANJUN RAN,[1,2] ZIKAI CHEN,[1,2] ZHIYONG BAI,[1,2,*] CHUROU HUANG,[1,2] ZHENG HUANG,[1,2] GUOXUAN ZHU,[1,2] CHANGRUI LIAO,[1,2] AND YIPING WANG[1,2]

[1]Key Laboratory of Optoelectronic Devices and Systems of Ministry of Education/Guangdong Province, College of Physics and Optoelectronic Engineering, Shenzhen University, Shenzhen 518060, China
[2]Shenzhen Key Laboratory of Photonic Devices and Sensing Systems for Internet of Things, Guangdong and Hong Kong Joint Research Centre for Optical Fibre Sensors, Shenzhen University, Shenzhen 518060, China
[3]Equal contributors.
*baizhiyong@szu.edu.cn

Abstract: We experimentally demonstrated an all-fiber reflective orbital angular momentum (OAM) generator based on orthogonal fiber Bragg grating (OFBG). The OFBG is formed by using a femtosecond laser to prepare two fiber Bragg gratings with a certain spacing in orthogonal planes. The ±1st- and ±2nd-order OAM modes were directly excited in this OFBG, and the chirality of the OAM modes depends on the relative positions of the two FBGs. The mode coupling properties and effects of center-to-center distance on OAM modes were investigated as well.

1. Introduction

In recent years, vortex beams carrying orbital angular momentum (OAM) have received more and more attention, and the helical phase in their electric field expression can be described as exp($il\varphi$), where l and φ are the topological charge and azimuth angle, respectively [1,2]. The phase singularity at the center of the OAM beam causes the mode field profile a doughnut-like shape [3]. Meanwhile, the OAM beams with different topological charges are naturally orthogonal. As a result, OAM beams are widely used in the fields of optical communication [4], optical tweezers [5], super-resolution microscopy [6], and sensing [7].

Currently, there are many devices and artificial nano/micro-structures used to generate OAM beams, including spiral phase plates [8], cylindrical lens mode converters [9], Q-plates [10], spatial light modulators [11], metasurfaces [12], fiber-tip microstructures [13,14], fiber gratings [15–21]. Among them, the OAM mode generation method based on fiber grating has attracted extensive attention of researchers due to its advantages of high conversion efficiency, high purity, flexible wavelength selectivity, and being completely compatible with fiber systems. FBG can realize the coupling of reverse transmission modes, and has a very narrow bandwidth which plays the role of a narrow-band high reflectivity mirror in the laser system. In addition, few/multi-modes FBG can realize the coupling of multiple modes in a smaller wavelength range which has potential for application to modular division multiplexing systems. In 2000, K. S. Lee and T. Erdogan theoretically verified that the simultaneous writing of FBGs with different inclination directions on an optical fiber can achieve simultaneous coupling of $LP_{01} \rightarrow LP_{11}^{e}/LP_{11}^{o}$, and the output light field has a circular distribution when the phase difference between the two FBGs is $(m+1/2)\pi$ [22]. In 2014, Lin et al. proposed a helical fiber Bragg grating: when a helical index modulation realized in few-mode fiber core, there would be a $\pi/2$ phase shift between HE_{21}^{e} and HE_{21}^{o} generated by horizontal and vertically coupling respectively, and it will result in the OAM mode [23]. In 2021, Z. Liu fabricated orthogonal long period fiber gratings to realize direct excitation of

#467491 https://doi.org/10.1364/OE.467491
Journal © 2022 Received 9 Jun 2022; revised 5 Jul 2022; accepted 5 Jul 2022; published 20 Jul 2022

Optics EXPRESS

OAM modes [17]. Compared with tilted FBG which requires the use of a polarization controller to generate OAM mode indirectly [18] and helical grating which requires complex systems and procedures for fabrication [16,20], orthogonal long period fiber grating is a simpler and more convenient all-fiber OAM modes generation. To the best of our knowledge, there is no experimental study using orthogonal fiber Bragg grating (OFBG) to generate OAM mode.

In this study, we achieved an OFBG to directly excite high-order OAM mode in four-mode fibers. The characteristics of the mode coupling and the effect of the center-to-center distance of mutually orthogonal FBG components on the OAM mode are studied. The results show that the proposed OFBG can directly generate the $\pm1^{st}$- and $\pm2^{nd}$-order OAM modes without any other devices and the conversion effect of OAM mode is the best when the phase difference is close to (m+1/2)π (where m is an arbitrary integer). In addition, OFBG has the advantage of low polarization dependent loss.

2. OFBG fabrication and spectral characteristics

The operation principle of OFBG directly exciting the OAM mode is shown in Fig. 1. FBG_1 located in the X and FBG_2 located in the Y directions couple the forward propagating LP_{01} mode to the reverse propagating LP^e_μ and LP^o_ν modes, respectively, where $\mu, \upsilon \in \{01,11,21,02\}$. When the phase difference between the reflected modes of the two gratings is (m+1/2)π, the OAM modes will be reflected. And the phase difference Δφ between modes in an OFBG is determined by the mode propagation constant β and the center-to-center distance ΔD of the two FBGs:

$$\Delta\varphi = (\beta_\mu + \beta_\upsilon)\Delta \mathrm{D} \tag{1}$$

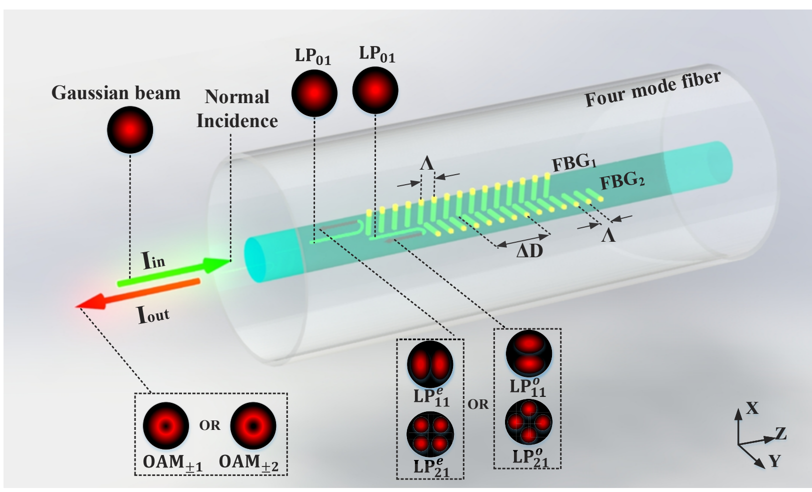

Fig. 1. Schematic diagram of OFBG directly generating OAM modes. ΔD: center-to-center distance between FBG1 and FBG_2; The green arrow indicates the propagation direction of the LP_{01}; The red arrow indicates the propagation direction of LP^e_{11}/LP^e_{21}, LP^o_{11}/LP^o_{21} and $OAM_{\pm1}/OAM_{\pm2}$.

Equation (1) combined with the phase matching condition of FBG can be simplified as:

$$\Delta\varphi = \frac{2\pi}{\Lambda}\Delta \mathrm{D} \tag{2}$$

where Λ is the pitch of the grating. Therefore, the Δφ between the modes reflected by the two gratings can be controlled by designing the ΔD of FBG_1 and FBG_2, and while it is (m+1/2)π, the $\pm1^{st}$-order OAM and $\pm2^{nd}$-order OAM modes will be output.

Optics EXPRESS

In this study, we used a four-mode step index fiber (YOFC) with core and cladding diameters of 18.5μm and 125μm, and refractive indices of 1.46183 and 1.45601, respectively, which can support LP_{01}, LP_{11}, LP_{21} and LP_{02} modes long-distance transmission theoretically. A femtosecond laser (PHAROS, 513nm/290fs/200kHz) was used to inscribe the FBG by line-by-line scanning. The femtosecond laser was focused using a 100× oil immersion objective with a numerical aperture of 1.25, and a matching oil with refractive index of 1.45 used to eliminate the cylindrical lens effect. The micrograph of FBG_1 as shown in Fig. 2(a_1) and (b_1), the length L of the line is set to 8 μm and the processing position is placed at the edge of the axial section of the fiber core to excite the asymmetric core mode and increase the coupling efficiency of high-order modes. The processing parameters of FBG_1 and FBG_2 are the same, whose grating pitch Λ =1.07μm, the number of periods n = 1400, and the single-pulse laser energy p = 4.76nJ. In order to ensure the consistency of process parameters and grating modulation, a femtosecond laser with a power stability of 0.5%rms over 100 h and a 3D-translation stage with an accuracy of 1 nm were used in this work. The specific preparation steps of OFBG are as follows. First, the FBG_1 was inscribed in a line-by-line scanning mode. Then, the fiber was rotated 90° by rotating fiber holder, and the micrographs were shown in Fig. 2(a_2) and (b_2). Next, the fiber was axially translated to the starting position of FBG_2, which is 0.3μm away from that of FBG_1. It is noted that $\Delta D = 0.3$μm is the optimal distance that the machining system can achieve to produce a phase difference closest to 0.5π, and the phase difference is 0.56π. Finally, repeated the first step to complete the preparation. The result was shown in Fig. 2(a_3) and (b_3) that the plane where FBG_2 is located is perpendicular to the plane where FBG_1 is located. During the preparation of OFBG, a spectrometer and a broadband light source used to monitor the spectrum of OFBG real-time.

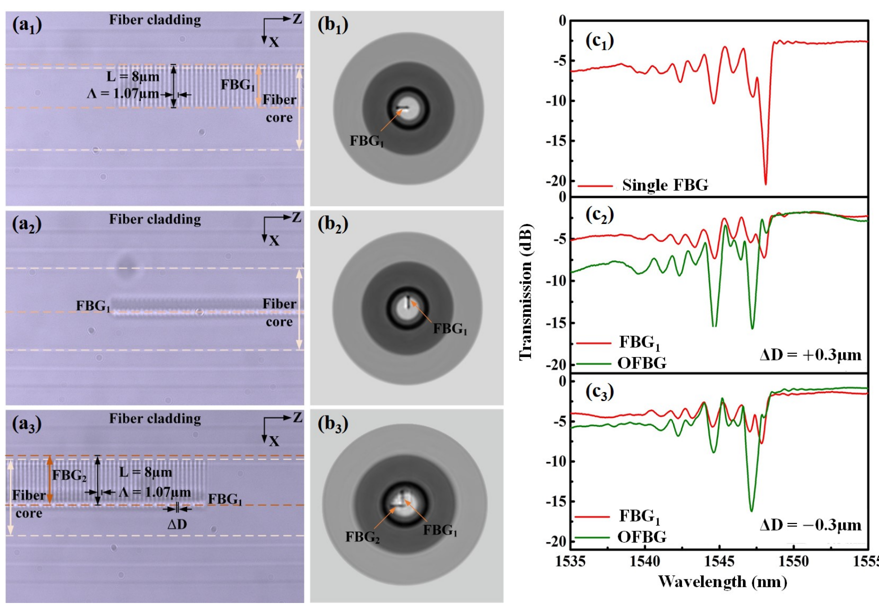

Fig. 2. (a_1) Micrograph after preparation of FBG_1; (a_2) Micrograph of FBG1 rotated 90 degrees in the state of (a_1); (a_3) Micrograph after preparation of FBG_2; (b_1), (b_2) and (b_3) correspond to the side micrographs in the states of (a); (c_1) Transmission spectrum of single FBG; (c_2) Transmission spectrum of OFBG with $\Delta D = +0.3$μm; (c_3) Transmission spectrum of an OFBG with $\Delta D = -0.3$μm.

The transmission spectra of OFBGs are shown in Fig. 2(c_2), (c_3). Compared with the FBG_1 (red line), the wavelength of the resonance peak of OFBG has a little blue-shift, and the coupling

Optics EXPRESS

strength increases. In addition, we prepared a single FBG using the above-mentioned method to compare the properties of polarization and OAM mode generation with that of OFBGs. The preparation parameters of single FBG are Λ=1.07μm, n = 1400, p = 5.08nJ, and its transmission spectrum is shown in Fig. 2(c_1).

We used a polarization analysis system (Keysight) to test the polarization dependent loss (PDL) of OFBG. Figure 3(a) and (b) represent the TE\TM spectrum and PDL of single FBG and OFBG respectively. Among them, TE and TM represent the transmission spectrum of the two polarization states with the maximum and minimum output power, respectively. As we can see, the PDL of the single FBG is as high as 11.84dB, while the PDL of OFBG is only 2.12dB, which is at significantly lower level. This is because the refractive index modulation of single FBG is located on one side of the fiber core, which cause refractive index modulation asymmetric in the core cross-section, resulting in a large PDL. The orthometric modulation of OFBG reduces part of the asymmetry and thus reduces the PDL.

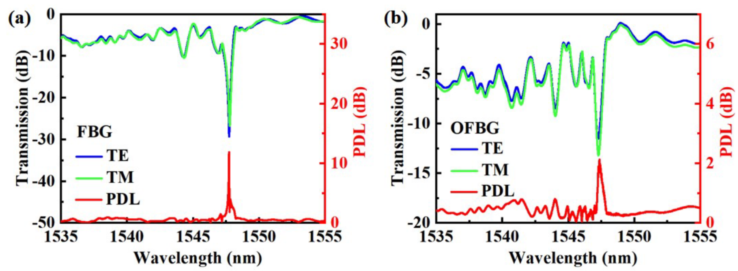

Fig. 3. TE\TM spectrum and PDL of (a) single FBG and (b) OFBG.

3. OAM generation characteristics

In order to explore the OAM mode generation characteristics of OFBG, we designed and built an OAM mode detection system as shown in Fig. 4, which can ensure that the OAM mode is excited by OFBG rather than the off-axis incidence of light using the principle of reversible optical path. The light beam from the tunable laser was collimated through a 10× objective lens, and then divided into two paths by beam splitter 1 (BS_1). One path of beam was reflected by BS_2, and then was normally incident into OFBG by a 20× objective lens. The OFBG coupled the incident fundamental mode to inverse light which met and coaxially interfered with the other path of beam at BS_3. Infrared camera (CCD) is used to observe intensity distribution of the coupled mode, and analysis phase information from the interference pattern. The attenuator located in the optical path is used to match the intensity of the two beams, and the polarizer located in front of the CCD is used to filter out background light which doesn't take part in interference, both of which is to improve the contrast of the interference fringes.

The mode intensity distributions at different resonance wavelengths were observed for single FBG and OFBGs with ΔD=±0.3μm (Δφ=±0.56π), as shown in Fig. 5(a). In OFBG, the donut-shape modes were obtained at resonant wavelengths of 1546.45nm, 1545.46nm for ΔD=+0.3μm, and at 1546.28nm, 1545.36nm for ΔD=-0.3μm. At the same time, LP_{01} and LP_{02} modes were respectively observed at the resonant wavelengths of 1547.22nm and 1544.98nm for ΔD=+0.3μm, and at 1547.20nm and 1545.00nm for ΔD=-0.3μm. For single FBG, LP_{01}, LP_{11}, LP_{21}, and LP_{02} modes were excited in the corresponding resonant wavelengths of 1547.26nm, 1546.66nm, 1545.42nm, and 1545.16nm, respectively. There was no donut-shaped mode presented in test processing.

The phase information of the donut-shape modes generated in OFBG was tested by using coaxial interference method, as shown in Fig. 6(a) and (b). The results show that, the spiral

Optics EXPRESS

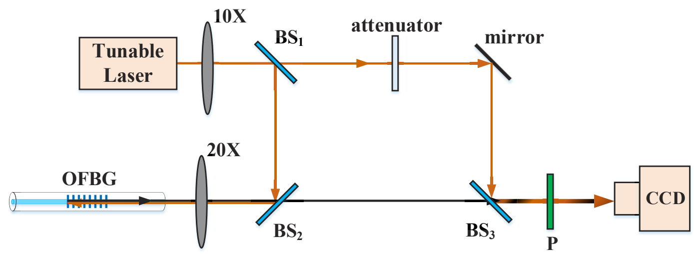

Fig. 4. Schematic diagram of OAM mode detection system (BS_1, BS_2 and BS_3: thin-film beam splitter; P: polarizer.)

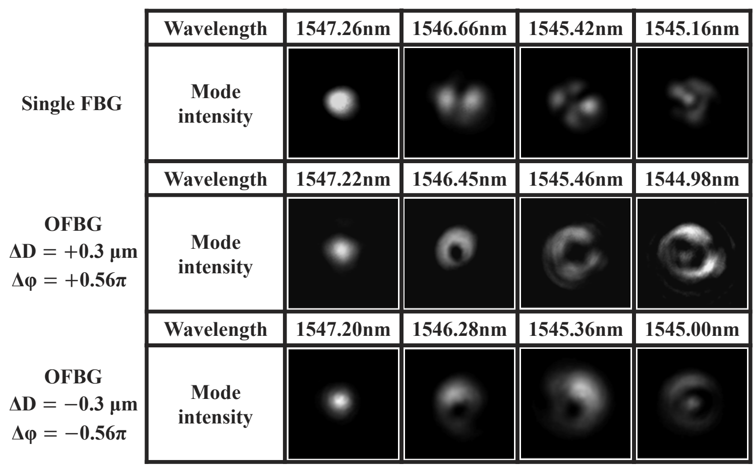

Fig. 5. Mode intensity distribution of single FBG and OFBG with $\Delta D = \pm 0.3\mu m$.

interference patterns were obtained, which indicated the excitation OAM modes. The topological charges of OAM modes were +1 and +2 for OFBG with ΔD=+0.3μm, and -1 and -2 for ΔD=-0.3μm. Thus, OFBG can directly generate OAM modes, and its topological charge can be controlled by combining ΔD and the wavelength of the incident light.

Using the above parameters and methods, OFBGs with ΔD of ±0.4μm ($\Delta\varphi = \pm 0.75\pi$) were prepared, and the intensity distribution and interference pattern of the coupled mode were tested at the resonant wavelength. The results show that the OFBGs still generated OAM modes with topological charges ±1 and ±2. However, the edges of mode profile and the spiral interference patterns are blurry, which indicated a decrease in mode purity. Thus, we can control the topological charge and quality of the OAM modes directly generated in OFBG by strictly controlling ΔD.

In this paper, the OFBGs has been realized to directly excite $\pm 1^{st}$ - and $\pm 2^{nd}$ –order OAM mode by introducing an interval ΔD between mutually orthogonal FBG components. When $\Delta\varphi$ induced by ΔD is close to ±π/2, the quality of the generated OAM mode is better. The OFBG is ease to fabrication since the spiral refractive index modulation is not required, and is flexible in application due to its direct generation of high-order OAM modes, narrow bandwidth and reflection-type. In addition, higher-order OAM mode can be realized by the OFBG as long as the optical fiber used can supports higher-order mode. This highly integrated device has a potential application in modular division multiplexing systems and vortex fiber laser.

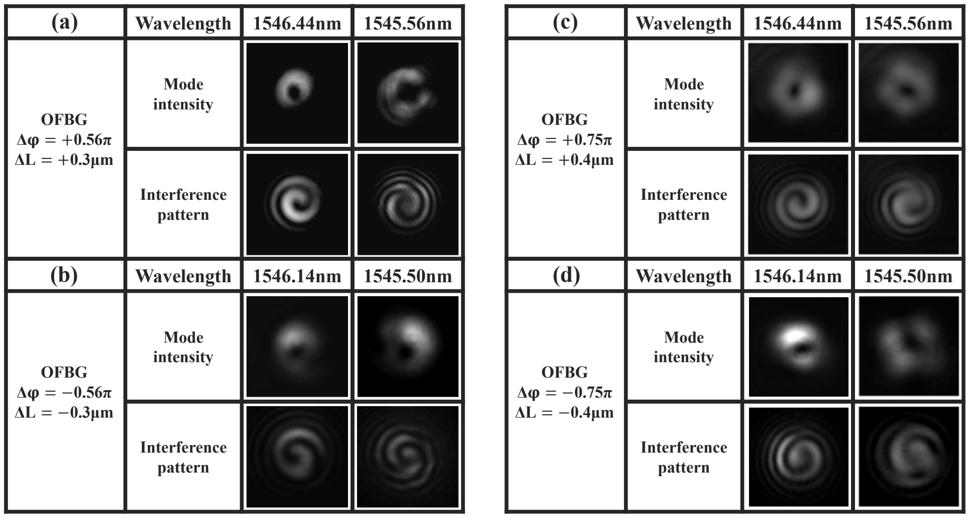

Fig. 6. Intensity and interferograms of OAM modes generated in OFBGs (a) and (b) with $\Delta\varphi = \pm 0.56\pi$; (c) and (d) with $\Delta\varphi = \pm 0.75\pi$.

Funding. Shenzhen University (2019097); Shenzhen Science and Technology Innovation Program (JCYJ20200109114201731); Natural Science Foundation of Guangdong Province (2022A1515010183); National Natural Science Foundation of China (61875134, 62005169).

Disclosures. The authors declare no conflicts of interest.

Data availability. Data underlying the results presented in this paper are not publicly available at this time but may be obtained from the authors upon reasonable request.

References

1. L. Allen, M. W. Beijersbergen, R. J. Spreeuw, and J. P. Woerdman, "Orbital angular momentum of light and the transformation of Laguerre-Gaussian laser modes," Phys. Rev. A **45**(11), 8185–8189 (1992).
2. J. Leach, S. Keen, M. J. Padgett, C. Saunter, and G. D. Love, "Direct measurement of the skew angle of the Poynting vector in a helically phased beam," Opt. Express **14**(25), 11919–11924 (2006).
3. A. M. Yao and M. J. Padgett, "Orbital angular momentum: origins, behavior and applications," Adv. Opt. Photonics **3**(1), 1 (2011).
4. N. Bozinovic, Y. Yue, Y. Ren, M. Tur, P. Kristensen, H. Huang, A. E. Willner, and S. Ramachandran, "Terabit-scale orbital angular momentum mode division multiplexing in fibers," Science **340**(6140), 1545–1548 (2013).
5. S.-Y. Huang, G.-L. Zhang, Q. Wang, M. Wang, C. Tu, Y. Li, and H.-T. Wang, "Spin-to-orbital angular momentum conversion via light intensity gradient," Optica **8**(1), 1 (2021).
6. L. Yan, P. Gregg, E. Karimi, A. Rubano, L. Marrucci, R. Boyd, and S. Ramachandran, "Q-plate enabled spectrally diverse orbital-angular-momentum conversion for stimulated emission depletion microscopy," Optica **2**(1), 1 (2015).
7. D. Deng, H. Zhao, J. Ni, Y. Li, and C.-W. Qiu, "A phase-to-intensity strategy of angular velocity measurement based on photonic orbital angular momentum," Nanophotonics **11**(4), 865–872 (2022).
8. M. W. Beijersbergen, R. P. C. Coerwinkel, M. Kristensen, and J. P. Woerdman, "HELICAL-WAVE-FRONT LASER-BEAMS PRODUCED WITH A SPIRAL PHASEPLATE," Opt. Commun. **112**(5-6), 321–327 (1994).
9. J. Courtial and M. J. Padgett, "Performance of a cylindrical lens mode converter for producing Laguerre-Gaussian laser modes," Opt. Commun. **159**(1-3), 13–18 (1999).
10. L. Marrucci, E. Karimi, S. Slussarenko, B. Piccirillo, E. Santamato, E. Nagali, and F. Sciarrino, "Spin-to-orbital conversion of the angular momentum of light and its classical and quantum applications," J. Opt. **13**(6), 064001 (2011).
11. M. T. Gruneisen, W. A. Miller, R. C. Dymale, and A. M. Sweiti, "Holographic generation of complex fields with spatial light modulators: Application to quantum key distribution," Appl. Opt. **47**(4), A32–A42 (2008).
12. X. Li, M. Pu, Z. Zhao, X. Ma, J. Jin, Y. Wang, P. Gao, and X. Luo, "Catenary nanostructures as compact Bessel beam generators," Sci. Rep. **6**(1), 20524 (2016).
13. Z. Xie, S. Gao, T. Lei, S. Feng, Y. Zhang, F. Li, J. Zhang, Z. Li, and X. Yuan, "Integrated (de)multiplexer for orbital angular momentum fiber communication," Photonics Res. **6**(7), 1 (2018).
14. J. Yu, Y.-P. Wang, W. Yang, Z.-Y. Bai, Z. Xie, Z. Liu, and C.-R. Liao, "All-fiber focused beam generator integrated on an optical fiber tip," Appl. Phys. Lett. **116**, 1 (2020).

Optics EXPRESS

15. Y. Zhao, C. Wang, Z. Liu, K. Zhou, C. Mou, Y. Liu, L. Zhang, T. Wang, and Ieee, "Generation of Multiple-Order OAM modes using a tilted Few-mode Fiber Bragg Grating," in *Asia Communications and Photonics Conference (ACP), Asia Communications and Photonics Conference and Exhibition* 2017.
16. H. Zhao, P. Wang, T. Yamakawa, and H. Li, "All-fiber second-order orbital angular momentum generator based on a single-helix helical fiber grating," Opt. Lett. **44**(21), 5370–5373 (2019).
17. Z. Liu, G. Zhu, Y. Li, J. Yu, Z. Bai, S. Liu, J. He, and Y. Wang, "Orthogonal long-period fiber grating for directly exciting the orbital angular momentum," Opt. Express **28**(18), 27044–27051 (2020).
18. K. Yang, Y.-G. Liu, Z. Wang, Y. Li, Y. Han, H.-W. Zhang, and B.-W. Mao, "Triple-order Orbital-angular-momentum modes generation based on single tilted fiber Bragg grating in a few-mode ring-core fiber," Opt. Fiber Technol. **55**, 1 (2020).
19. Y. Li, Z. Bai, Z. Liu, G. Zhu, K. Yang, J. Yu, J. Chen, C. Fu, C. Liao, and Y. Wang, "High purity optical vortex generation in a fiber Bragg grating inscribed by a femtosecond laser," Opt. Lett. **45**(24), 6679–6682 (2020).
20. Z. Huang, Z. Bai, G. Zhu, C. Huang, J. Chen, S. Liu, C. Fu, J. He, and Y. Wang, "Excitation of high order orbital angular momentum modes in ultra-short chiral long period fiber gratings," Opt. Express **29**(24), 39384–39394 (2021).
21. J. Chen, Z. Bai, G. Zhu, R. Liu, C. Huang, Z. Huang, L. Wu, C. Liao, and Y. Wang, "Femtosecond laser inscribed helical long period fiber grating for exciting orbital angular momentum," Opt. Express **30**(3), 4402–4411 (2022).
22. K. S. Lee and T. Erdogan, "Fiber mode conversion with tilted gratings in an optical fiber," J. Opt. Soc. Am. A **18**(5), 1176–1185 (2001).
23. Z. Lin, A. Wang, L. Xu, X. Zhang, B. Sun, C. Gu, and H. Ming, "Generation of Optical Vortices Using a Helical Fiber Bragg Grating," J. Lightwave Technol. **32**(11), 2152–2156 (2014).